Journal of Renewable Materials

Tech Science Press

DOI: 10.32604/jrm.2022.022659

ARTICLE

Effects of Strain Rate and Fiber Content on the Dynamic Mechanical Properties of Sisal Fiber Cement-Based Composites

Yubo Zhang, Ping Lei, Lina Wang and Jiqing Yang*

Facuty of Architecture and Civil Engineering, Yunnan Agricultural University, Kunming, 650000, China

*Corresponding Author: Jiqing Yang. Email: yjq.98@163.com

Received: 19 March 2022 Accepted: 22 May 2022

ABSTRACT

In this paper, a split Hopkinson pressure bar (SHPB) was used to investigate the dynamic impact mechanical behavior of sisal fiber-reinforced cement-based composites (SFRCCs), and the microscopic damage evolution of the composites was analyzed by scanning electron microscopy (SEM) and energy-dispersive X-ray spectrometry (EDS). The results show that the addition of sisal fibers improves the impact resistance of cement-based composite materials. Compared with ordinary cement-based composites (OCCs), the SFRCCs demonstrate higher post-peak strength, ductility, and energy absorption capacity with higher fiber content. Moreover, the SFRCCs are strain rate sensitive materials, and their peak stress, ultimate strain, and energy integrals all increase with increasing strain rate. From the perspective of fracture failure characteristics, the failure of OCCs is dominated by the brittle failure of crystal cleavage. In contrast, the failure mode of the SFRCCs changes to microscale matrix cracks, multi-scale pull-out interface debonding of fibers (fine filaments and bundles), and mechanical interlock. This research provides an experimental basis for the engineering application of high-performance and green cement-based composites.

KEYWORDS

Sisal fiber; cement-based composites; SHPB; energy integration; microstructure damage evolution law

1 Introduction

At present, cement-based composites are the most commonly used building materials in the world. The large-scale production and use have promoted the development of human production and infrastructure. However, cement has also led to significant resource consumption and environmental pollution [1]. With the continuous development of human civilization and its dependence on industry, negative factors such as the depletion of energy resources and the hazardous impact of carbon emissions are gradually being highlighted. Therefore, resource consumption and environmental issues have become crucial issues that affect the selection of engineering materials.

The introduction of natural or artificial fibers into cement can improve the tensile performance, crack resistance, and durability of cement-based composites [2] in addition to the reduction of resource consumption and environmental pollution. Therefore, this strategy is beneficial for the sustainable development due to the ability to decrease carbon emissions and the cost of construction materials [3,4]. There are various types of fibers with specific performance that play different roles in cement-based

materials [5]. Based on their peculiar characteristics, fibers are categorized as metal fibers, synthetic fibers, mineral fibers, and natural fibers [6,7]. Compared to man-made fibers, the natural fiber not only exhibits the higher specific modulus and specific strength, but also some degradable characteristics, the possibility of being extracted from renewable sources, low cost, and non-toxicity. Among natural fibers, preference is given to plant fibers such as coir, hemp, bamboo, jute, flax, ramie, sisal, bagasse, and specialty fibers obtained via wood processing [8]. However, unlike most plant fibers, sisal fibers are resistant to friction, corrosion, very high or low temperatures, and humidity [9]. Therefore, in recent years, considerable attention has been paid to renewable sisal fibers [10–14].

The popularization and application of sisal fiber-reinforced cement-based composites (SFRCCs) have broadened the comprehensive utilization of sisal biological resources and reduced the consumption of polypropylene, polyvinyl alcohol fiber, carbon fiber, glass fiber, steel fiber, and cement in composites. Therefore, SFRCCs have the dual significance of efficient resource utilization and good environmental protection, which has led to widespread interest in them [13,15,16]. In normal use, building structures are inevitably subjected to accidental impacts, which may cause local component and structure damage or even total structure collapse. However, although the quasi-static mechanical properties of SFRCCs have been reported [17], the research on their dynamic mechanical properties is still relatively limited. Therefore, achieving a comprehensive understanding of the dynamic mechanical properties and toughening mechanisms of SFRCCs is of great importance.

The dynamic mechanical behavior of concrete can be characterized by various methods, including drop hammer impact [18], projectile penetration impact [19,20], split Hopkinson pressure bar (SHPB) [21,22], and explosive shock [23], according to the dynamic impact strain rate range. Among these techniques, drop hammer impact and projectile penetration impact are usually used to analyze the damage evolution characteristics of materials under dynamic loading. However, SHPB systems allow one to simultaneously analyze the dynamic impact damage evolution and the dynamic stress-strain response of materials, allowing for the characterization of their dynamic mechanical behavior. Huang et al. [24] studied the dynamic compression mechanical properties of lightweight aggregate concrete using a 155 mm diameter SHPB system. They concluded that the dynamic strength and magnitude of the energy absorption density generally increased with increasing impact velocity for strain rates ranging from 40 to 140 s^{-1}. According to Trindade et al. [25], strain-hardening geopolymer composites fabricated with molecular-weight polyethylene fibers exhibited superior mechanical performance compared to a composite made with PVA fibers.

In practical engineering applications, structural design is closely related to the complete stress-strain response of a material. For different composite systems, researchers have proposed different stress-strain curve analyses and prediction models. Abadel et al. [26] used three models to investigate the stress-strain curve of hybrid fiber-reinforced cement (HFRC) based composites (with hooked-ended steel, crimped polypropylene, or plain Kevlar fibers). They quantified the influence of the fibers on the compressive and tensile strength, stress-strain curves, and flexural toughness ratio of the HFRCs according to the fiber reinforcement index. Cao et al. [27] studied the effect of steel-PVA hybrid fibers on the stress-strain full curve and compressive behavior of $CaCO_3$ whisker-reinforced cement mortar. They proposed compressive parameter prediction models by simultaneously considering the reinforcing index (RI) of the steel and PVA fibers. Khan et al. [28] developed the compressive models to describe the experimental stress-strain curves of basalt-steel fiber-$CaCO_3$ whisker reinforced fly ash concrete (BSC-FAC). The proposed analytical fitting models showed good coincidence with the experimental data.

In this paper, the dynamic mechanical behavior of SFRCCs at different strain rates and fiber contents was studied by using an SHPB device. Scanning electron microscopy (SEM) was applied to explore the fiber strengthening and toughening mechanism of a cement matrix at the microscale. The stress-strain

curves were established, and a dynamic constitutive law was established for the SFRCC materials under impact loading. The results of this work would be beneficial for further improvement of the performance of SFRCCs with appropriate fiber contents, thereby providing a theoretical basis and a further guidance for engineering application of these materials under the influence of dynamic impact loads.

2 Materials and Method

2.1 Raw Materials

The composition of the SFRCCs used in this experiment mainly included cement, fine aggregate, sisal fiber, water, and a water-reducing agent.

(1) The cement was ordinary Portland cement (P.O 42.5) produced by Nujiang Kungang Cement Co., Ltd. (China). Its main performance indicators are shown in Table 1.
(2) The fine aggregate was machine-made sand in the range of 0 to 4.75 mm. Its various performance indicators are listed in Table 2.
(3) The admixture used in this experiment was a retarding type high-performance polycarboxylic acid water reducer (high strength). The main physical properties of the admixture are shown in Table 3.
(4) The sisal fiber precursor was produced by Guangxi Agricultural Reclamation State-owned Shanwei Farm. This precursor was chopped to a length of (10 ± 1) mm. The fiber morphology and microstructural characteristics of the fiber are provided in Fig. 1 and its mechanical parameters can be found in Table 4.
(5) Ordinary laboratory tap water was used in this experiment.

Table 1: Physical and mechanical properties of cement

Parameter	Setting time (min)		Stability (mm)	Strength at 28 d (MPa)	
	Initial setting	Final setting		Anti-bending	Compressive
Index value	132	208	0.5	8.2	44.9
Technical requirement	≥45 min	≤600 min	≤5.0	≥6.5	≥42.5

Table 2: Performance indicators of fine aggregate

Parameter	Fineness modulus	MB	Mud content (%)	Crush index (%)
Index value	2.8	6.3 (MB = 0.8)	0.0	22
Technical requirement	2.3–3.0	≤7.0	≤1.0	<25

Table 3: Performance indicators of additives

Parameter	Water reduction rate (%)	Bleeding rate ratio (%)	Initial setting time (min)	pH value
Index value	31	21	+130	6.01
Technical requirement	≥25	≤70	>+90	/

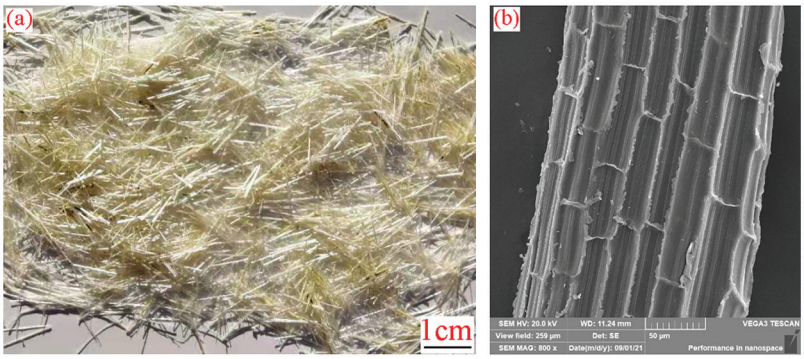

Figure 1: (a) Chopped sisal fiber and (b) Microstructure morphology of sisal fiber

Table 4: Mechanical parameters of the sisal fiber

Place of origin	Density (kg/m³)	Tensile strength (MPa)	Elongation percentage (%)
Guangxi agricultural reclamation state-owned shanwei farm	1295	510	6.0

2.2 Cement Mix Design

Cement was mixed according to JGJ/T 221–2010 standard "Technical Regulations for the Application of Fiber Concrete". The sisal fiber content in the cement was 0 vol%, 0.1 vol%, or 0.2 vol%, and a water-cement ratio of 0.33 was used. The specific mix ratios are shown in Table 5. The obtained fiber-reinforced cement-based composites were labeled PC, SF1%vol, and SF2%vol.

Table 5: Mixing ratio of cement-based composites

Sample	Cement (kg/m^3)	Sand (kg/m^3)	Water (kg/m^3)	Water-reducing agent (kg/m^3)	Sisal fiber content (%)
PC	702	702	246	4.2	0
SF1%vol	702	702	246	4.2	1
SF2%vol	702	702	246	4.2	2

2.3 Experimental

2.3.1 Preparation of Cement-Based Composites

First, the raw materials were stirred together, as shown in Fig. 2. After being poured into the mold, each mixture was fully vibrated (refer to Fig. 3 for more details). Second, the specimens were demolded after 24 h of initial setting and cured for 28 days in a curing room at a temperature of (20 ± 2)°C and the humidity higher than 95%. Third, the cured specimens were cut into 3 pieces and polished. The flatness of the end face was kept within 0.1 mm. A sample used for testing is illustrated in Fig. 4.

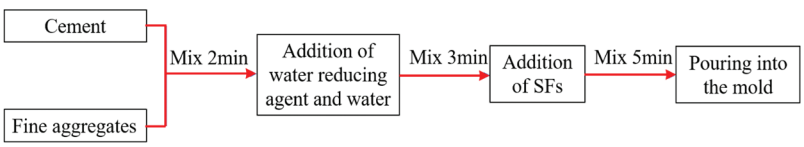

Figure 2: Cement-based composite mixing process

Figure 3: Composite pouring molding sample

Figure 4: Composite SHPB impact sample

2.3.2 Dynamic Mechanical Performance Testing

(1) Test principle

A Hopkinson pressure bar system (SHPB) (Fig. 5) was employed to investigate the dynamic mechanical properties of the SFRCCs. The test appliance was composed of a bullet, an incident rod, a transmission rod, a data acquisition system, and a nitrogen power device. The bullet, incident rod, and transmission rod were all 80 mm in diameter. Based on the one-dimensional elastic stress wave theory and assuming stress uniformity, the stress, strain, and strain rate of the specimens were obtained as follows [29]:

$$\sigma = \frac{A_{\mathrm{H}} E_{\mathrm{H}}}{A_S} \varepsilon_T \tag{1}$$

$$\varepsilon = -\frac{2c}{L} \int_0^t \varepsilon_R dt \tag{2}$$

$$\dot{\varepsilon} = -\frac{2c}{L} \varepsilon_R \tag{3}$$

where E_H, c, and A_H respectively represent the elastic modulus, wave velocity, and cross-sectional area of the compression rod. A_S and L are the cross-sectional area and length of the specimen and t is the time.

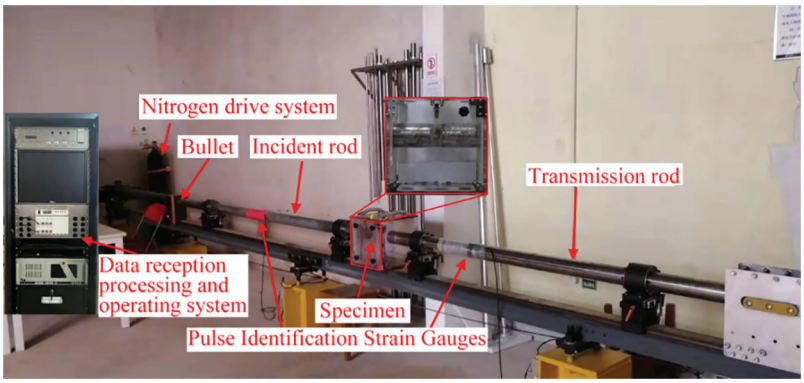

Figure 5: A SHPB test device

To analyze the dynamic energy absorption characteristics of the SFRCCs, the energy integration (energy absorbed per unit volume, or J) parameter was used [30]. It was obtained by integrating the stress-strain curve as follows:

$$J = \int_0^{\varepsilon_{max}} \sigma d\varepsilon \tag{4}$$

(2) Experimental procedure

Dynamic compression test specimens were cylindrical blocks with a designated size of ϕ 70 mm × H 35 mm. Three tests were performed under each test condition, and the two sets of results with a lower difference were selected for representation. To analyze the evolution relationship between the dynamic mechanical properties and fiber content of the specimens, their dynamic stress-strain curves were measured. Moreover, the stress-strain curves of SF2%vol were tested under two different impact air pressures (6 and 8 bar), with the aim of investigating the effect of strain rate on the dynamic mechanical properties. Combined with a fracture microstructure morphology analysis, a microstructure damage evolution law was established for the SFRCCs and the strengthening and toughening mechanisms of the sisal fibers were further discussed.

2.3.3 Microstructure Analysis

A TESCAN VEGA-3 scanning electron microscope (SEM) was used to probe the fracture microstructure of the SFRCCs with different fiber volume contents. Energy-dispersive X-ray spectrometry (EDS) was employed to analyze the physical and chemical properties at the points selected on the interface between the fiber and the cement paste in SF2%vol.

3 Results and Analysis

3.1 Dynamic Mechanical Behavior of SFRCCs with Different Fiber Contents

Fig. 6 depicts the dynamic stress-strain curves of the cement-based composites with different sisal fiber contents. The curves could be roughly divided into three stages. In the first stage, the stress sharply increases with increasing strain until it reaches a peak. In the second stage, the stress suddenly drops. In this stage, the stress initially decreases in a rapid manner and eventually stabilizes with increasing strain. The third stage is the strength residual stage. In this stage, the stress remains almost unchanged with increasing strain. Instead, the stress fluctuates and gradually decreases until the final failure is reached.

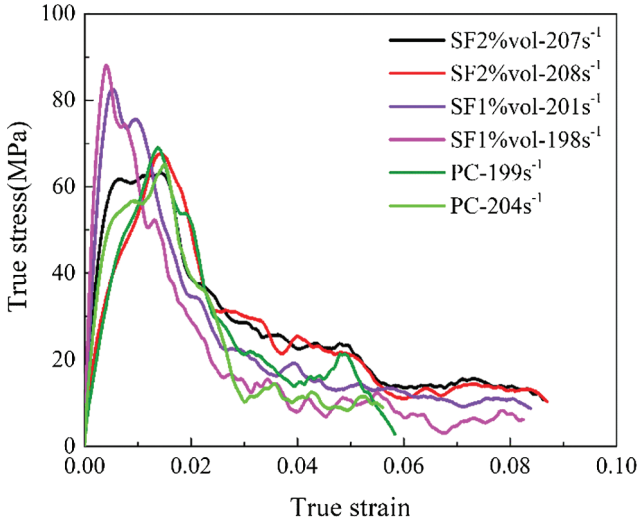

Figure 6: Stress-strain curves of cement-based composites with different fiber contents

In combination with the dynamic stress-strain characteristic values (Table 6), the effect of fiber content on the dynamic mechanical properties of the SFRCCs is clear. The highest peak stress is achieved with a fiber content of 1 vol%. When the fiber content is 2 vol%, the peak stress is equivalent to that of the OCCs. This is potentially because the higher fiber content leads to the intertwining and agglomeration, which limits the strengthening effect of the fibers. From the perspective of ultimate strain, the larger fiber content means the higher ultimate strain.

Table 6: Characteristic values of composites with different fiber contents

Material	Ultimate strain	Peak stress (MPa)	Energy integral ((1×10^6) J/m^3)
SF2%vol-207 s^{-1}	0.08645	63.30939	2.42118
SF2%vol-208 s^{-1}	0.08699	67.75534	2.30171
SF1%vol-201 s^{-1}	0.08388	82.59346	2.16512
SF1%vol-198 s^{-1}	0.08249	88.06695	1.77372
PC-199 s^{-1}	0.05836	69.09326	1.71795
PC-204 s^{-1}	0.05602	65.10803	1.54614

Energy integral (toughness) is an important index to describe the dynamic performance of materials, reflecting their ability to deform and absorb energy. Fig. 7 depicts a schematic representation of the material toughness (e.g., the area under the stress-strain curve [31]). This demonstrates that increasing the fiber content can significantly improve the impact mechanical properties of cement-based composites. Other relevant studies [32,33] have also reported that the introduction of plant fibers can reduce the density of cement-based composites, improve their flexural strength, inhibit and stabilize the development of microcracks, and enhance their impact resistance.

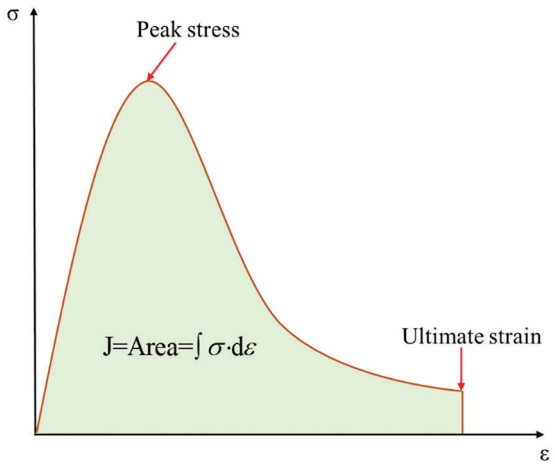

Figure 7: Schematic representation of material toughness, peak stress, and ultimate strain [31]

The residual strength of the composites significantly increases with increasing fiber content. According to the dynamic impact crushing morphology of these composites (Fig. 8), the crushing degree of the OCCs is more significant after dynamic compression than that of the SFRCCs. Furthermore, the higher fiber content results in a lower crushing degree. Therefore, these results confirm that the higher fiber content yields the

better residual mechanical properties in the later stage. This is mainly because the bridging effect of the fibers improves the impact toughness of the composites.

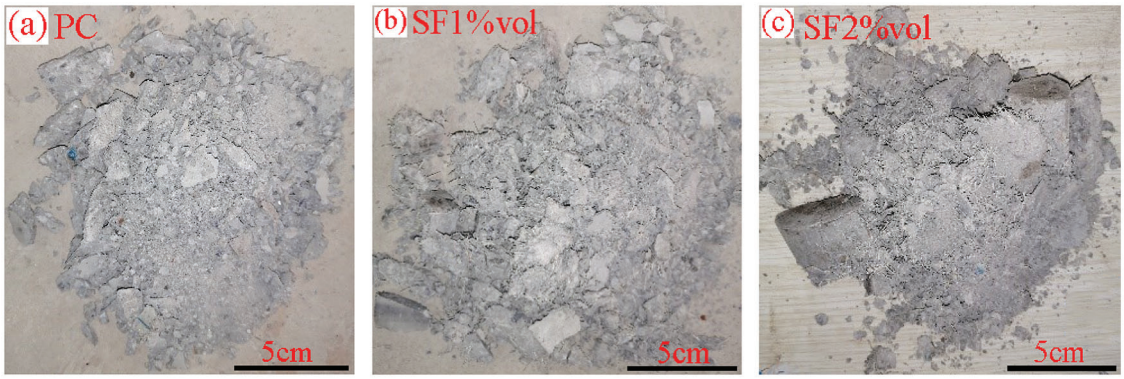

Figure 8: Crushing characteristics of cement-based composites with different fiber contents: (a) PC, (b) SF1%vol, and (c) SF2%vol

3.2 Dynamic Mechanical Behavior of SF2%vol Composite

Fig. 9 displays the stress-strain curves of SF2%vol under different strain rates. The peak stress and ultimate strain of this cement-based composite both increase with increasing strain rate, showing that the SFRCCs are strain rate sensitive materials. According to Table 7, the peak stress, ultimate strain, and energy integral of SF2%vol significantly increase with increasing strain rate. The dynamic impact morphology shown in Fig. 10 demonstrates that a higher strain rate results in more serious dynamic impact crushing, which can be explained by the plastic work absorption capacity of the material. That is, a higher strain rate yields the absorption of more plastic work by the composite, thereby increasing the impact crushing degree.

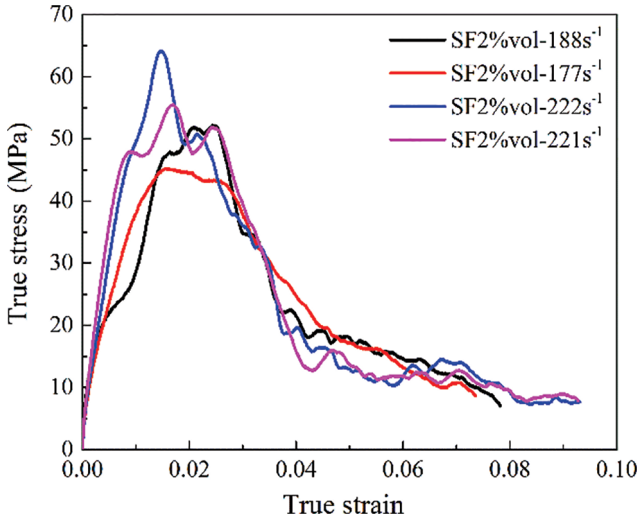

Figure 9: Stress-strain curves of SF2%vol at different strain rates

Table 7: Characteristic values of SF2%vol under different strain rates

Material	Ultimate strain	Peak stress (MPa)	Energy integral ((1×10^6) J/m^3)
SF2%vol-188 s^{-1}	0.07818	52.16630	1.95158
SF2%vol-177 s^{-1}	0.0735	45.25675	1.90130
SF2%vol-222 s^{-1}	0.09311	64.16738	2.19586
SF2%vol-221 s^{-1}	0.09281	55.50018	2.19609

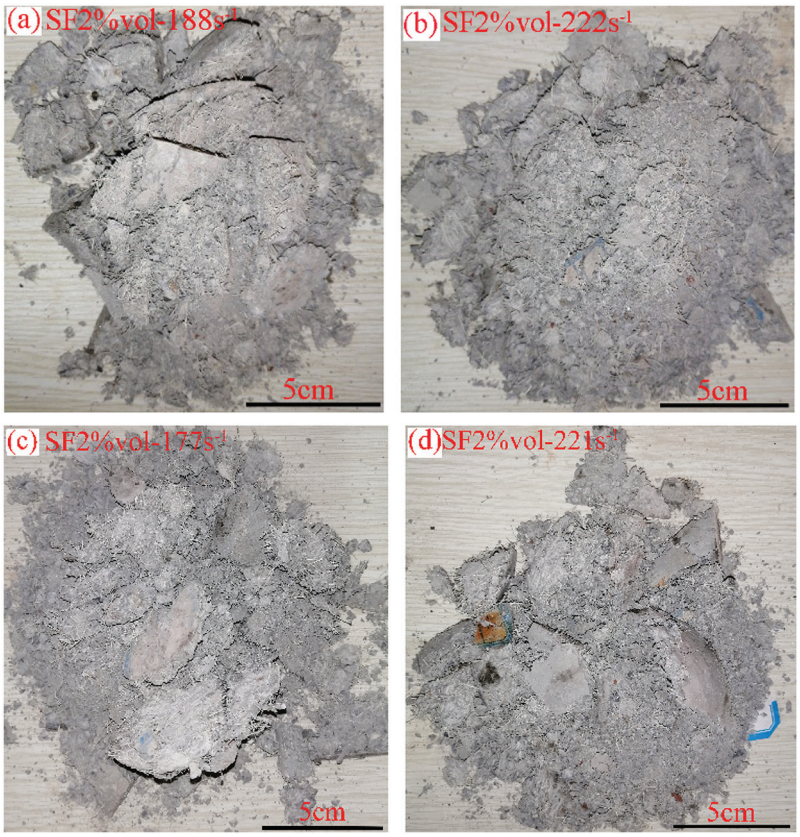

Figure 10: Crushing characteristics of composite SF2%vol at different strain rates

3.3 Strengthening and Toughening Mechanism of Sisal Fiber in Cement Matrix

Fig. 11 depicts the microstructure characteristics of the composite fracture morphology under a high strain rate. The fracture of the OCC is relatively flat, accompanied by voids and a cleavage shear plane of the hydration products. These characteristics show that the failure mode of the OCC composite is mainly brittle failure. In contrast, the stepped fracture of the SFRCCs is significant, whereas pull-out ends, pull-out traces, and holes in fibers are distributed across the entire fracture surface. In addition, the fibers are chaotically distributed and some of them are oriented perpendicular to the shear stress plane, leading to shear damage at the fiber roots and lodging on the fracture surface. Therefore, it can be concluded that the addition of fibers improves the toughness of these cement-based composites to a certain extent.

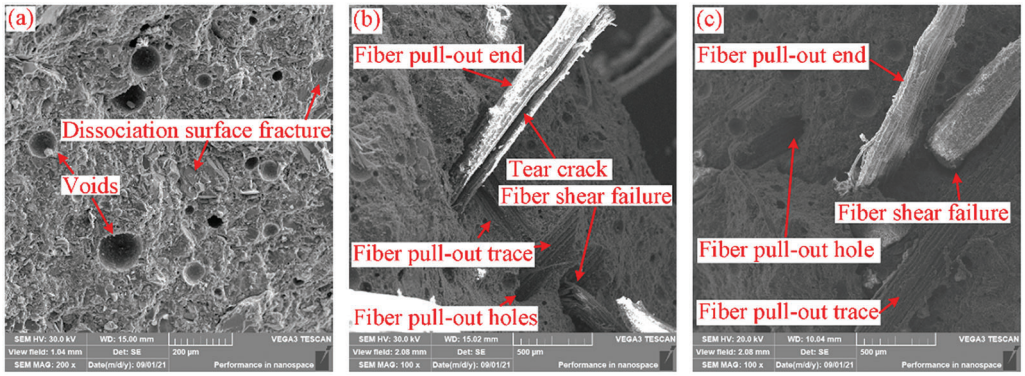

Figure 11: Dynamic fracture characteristics of cement-based composites: (a) PC, (b) SF1%vol, and (c) SF2%vol

Fig. 12 shows the local microstructure characteristics of the cement-based composite SF2%vol. The addition of the fiber changes the failure mode of these composites. Ones of the failure signatures observed in the SFRCCs are microcracks initiated at the interface between the fiber pull-out holes and followed by the crack propagation to voids, which leads to the formation of larger cracks until failure occurs (see Fig. 12a). Fig. 12b depicts the microstructure of the interface between the fibers and the cement matrix, which demonstrates that fibers are torn into micro-bundles under the impact load. The fibers and micro-bundles lead to the interface debonding failure at multiple scales, improving the impact resistance of the composites to a certain extent.

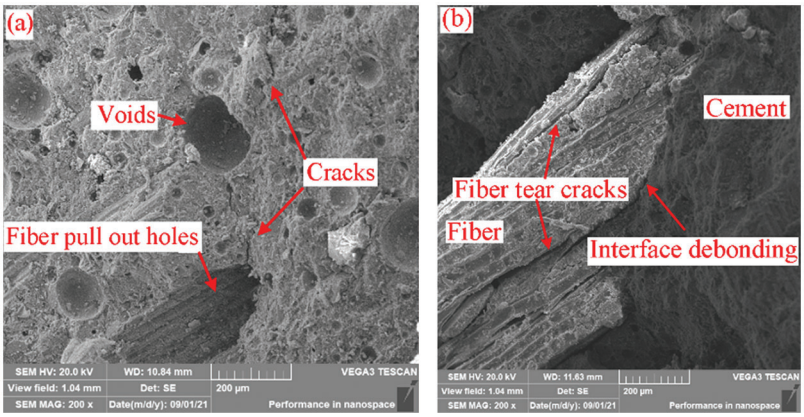

Figure 12: Failure microstructure of SF2%vol composite: (a) Microcrack propagation and (b) Multi-scale interface debonding

To verify the variation law of the composite interface physicochemical properties, sisal raw fibers and the interface between the fibers and the cement matrix in SF2%vol after impact were analyzed by EDS. The energy spectrum of the sisal fibers is shown in Fig. 13a. For the SF-2%vol interface zones, two points were selected: One on the fiber surface and the other in the cement, as shown in Fig. 13b. For comparison, the types and proportions of elements in these EDS-scanned areas were quantitatively analyzed (Table 8). Both analyzed points mainly show the presence of C and O, whose concentrations are about 32% and 69.8%, respectively. However, at points 3 and 4, the contents of C and O are 18.8% and 23%. Furthermore, Si and Al also appear at point 4 in concentrations of 7.5% and 1.6%, respectively. This is because the roughness of

the fiber surface leads to mechanical interlocking with the cement matrix. A part of the matrix therefore adheres to the fiber surface under impact loading, demonstrating that one of the strengthening and toughening mechanisms of sisal fibers is mechanical interlocking caused by the roughness of the fiber surface.

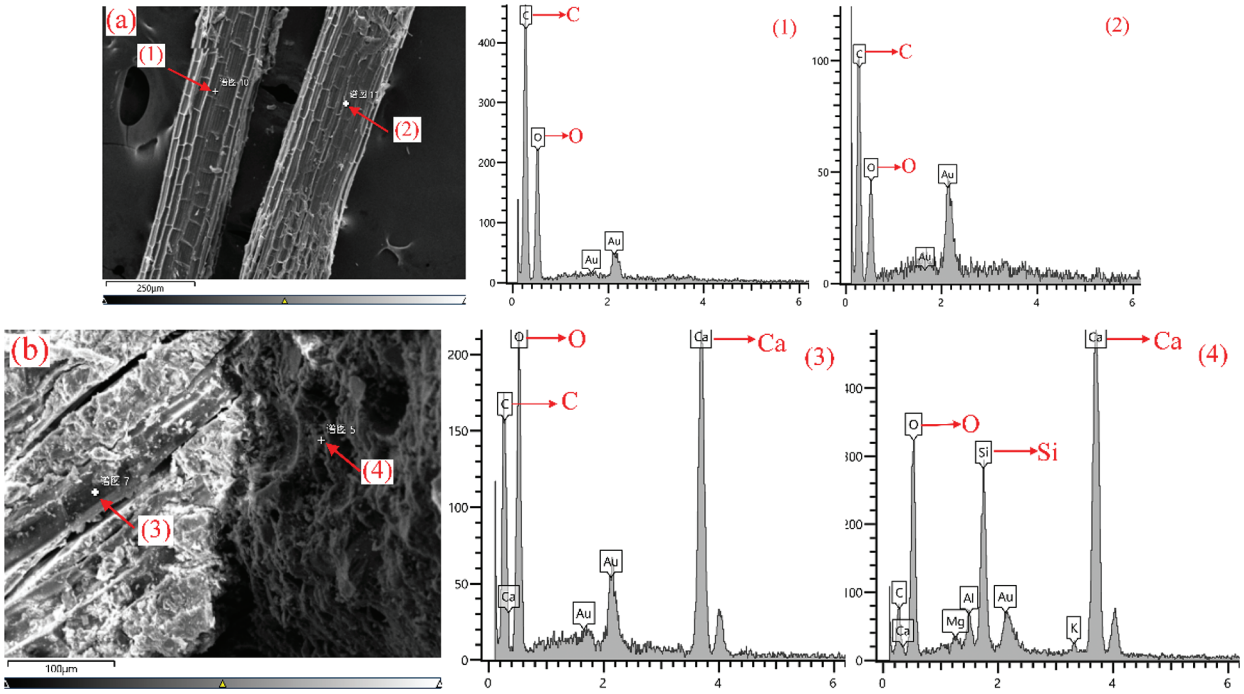

Figure 13: EDS analysis of (a) Sisal fibers and (b) The fiber-cement interface of SF2%vol

Table 8: Elemental analysis of SF2%vol

Element	C (%)	O (%)	Al (%)	Si (%)	Ca (%)
Spectrum 1	30.2	69.8	0	0	0
Spectrum 2	32.6	67.4	0	0	0
Spectrum 3	9.6	71.7	0	0	18.8
Spectrum 4	3.1	63.7	1.6	7.5	23.0

This analysis demonstrates that the addition of sisal fibers improves the dynamic impact resistance of cement-based composites to a certain extent. The strengthening and toughening mechanism is mainly based on the fiber bridging theory and the matrix microcracks, the multi-scale debonding of fibers (fibers and micro-bundles), and the mechanical interlocking caused by the fiber surface roughness.

3.4 Analysis of Dynamic Compressive Stress-Strain Relationship

The stress-strain relationship of fiber-reinforced composites is very important for structural engineering design, finite element calculations, and engineering applications. This is also the theoretical basis for using cement-based composites in engineering industries. Given the stress-strain relationships, the continuous mathematical models have been proposed for a variety of materials [26–28]. The empirical models for the stress–strain curves of cement-based composites can be divided into two categories: Those with

continuous functions combining the ascending and descending branches or separate functions for the two branches.

For the continuous functions, the most common models are [26,27]:

$$y = \frac{Cx + (D-1)x}{1+ (C-2)x + Dx^2} \tag{5}$$

$$y = \frac{Mx + (N-1)x^2}{1+ (M-2)x + Nx^2} \tag{6}$$

$$y = \frac{Lx}{L-1+ x^L} \tag{7}$$

where C, D, M, N, and L are the undetermined coefficients, whose specific values can be obtained by the nonlinear analysis of the stress-strain curves.

The two separate functions for the two branches are presented by a piecewise function consisting of a cubic parabola and a rational fraction, which can be employed to describe the ascending stage before the peak stress and the descending stage after the peak stress (X > 1), respectively, as follows [27]:

$$Y = hX + (3-2h)\mathrm{X}^2 + (h-2)X^3,\ 0 \le X \le 1 \tag{8}$$

$$Y = \frac{X}{k(X-1)^2 + X},\ X > 1 \tag{9}$$

However, modifications were made by some researchers in the compressive stress-strain curves because of the longer linear ascending branch due to the higher uniaxial compressive strength as follows [28]:

$$Y = c_1X + (5-4c_1)X^4 + (3c_1-2)X^5,\ 0 \le X \le 1 \tag{10}$$

The typical stress-strain curve of the composites is shown in Fig. 14. As is seen, the stress gradually increases with increasing strain until a peak stress is achieved. After the peak stress value is reached, the stress decreases with increasing strain. An inflection point that indicates a change in the curvature is observed from the descending branch of the curve. For mathematical convenience, the equations of normalized stress-strain curves were used to establish the dynamic stress-strain relationship of composites. In addition, the stress-strain curve must strictly meet the following mathematical criteria proposed by Guo [34]:

(1) The curve should pass through the origin, i.e., X = 0 and Y = 0;

(2) The slope of the stress-strain ascending branch must decrease monotonically, when 0 ≤ X < 1;

(3) The slope should be equal to zero at the maximum point where the X = 1 and Y = 1.

In this paper, the continuous functions were selected to analyze the dynamic impact stress-strain behavior of the SFRCCs, and the validity of the fitting results was verified in strict accordance with the above mathematical boundary conditions.

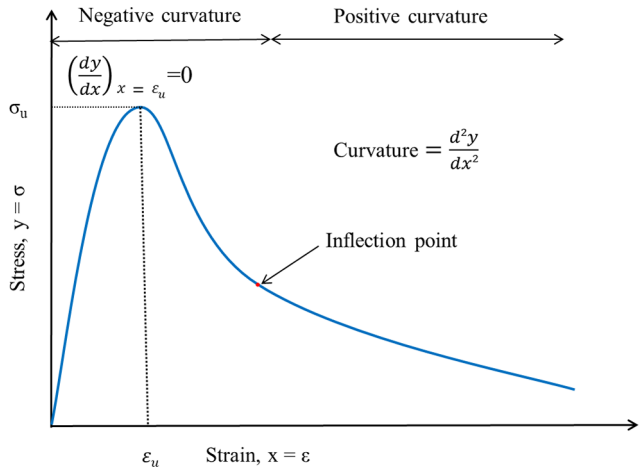

Figure 14: Typical uniaxial compressive stress-strain curves of the cement-based composites [27]

3.4.1 Construction of Dynamic Stress-Strain Relationship Models

The SFRCC dynamic stress-strain models are shown in Eqs. (5), (6), and (7) and are denoted as model 1, model 2, and model 3, respectively. The nonlinear analysis results are presented in Fig. 15. According to these data, all three models effectively fit the experimental curves and the fitting variance of model 1 is significantly better than those of model 2 and model 3.

3.4.2 Validation of the Dynamic Stress-Strain Curve Models

In addition to consistency between the fitting curve and the test results, the composite stress-strain relationship models should also strictly meet the model boundary conditions. The control points of the boundary conditions are the first derivative and the second derivative of the curve origin (x = 0) and the peak stress point (x = 1). The expression and validity verification are shown in Table 9. Although the simulation results of model 1 and model 2 are consistent with the experimental data, they fail to fulfil the requirements of mathematical significance. In contrast, model 3 meets the stringent mathematical boundary conditions of the whole curve. Therefore, the stress-strain relationship of the cement-based composites reported in this paper can only be described by model 3. Furthermore, the index L analysis of model 3 in Fig. 15 reveals that the index L trend is opposite to those of the peak stress for the composites with different fiber contents, indicating that model 3 reflects the contribution of fiber content to the peak stress of the SFRCCs under the dynamic impact.

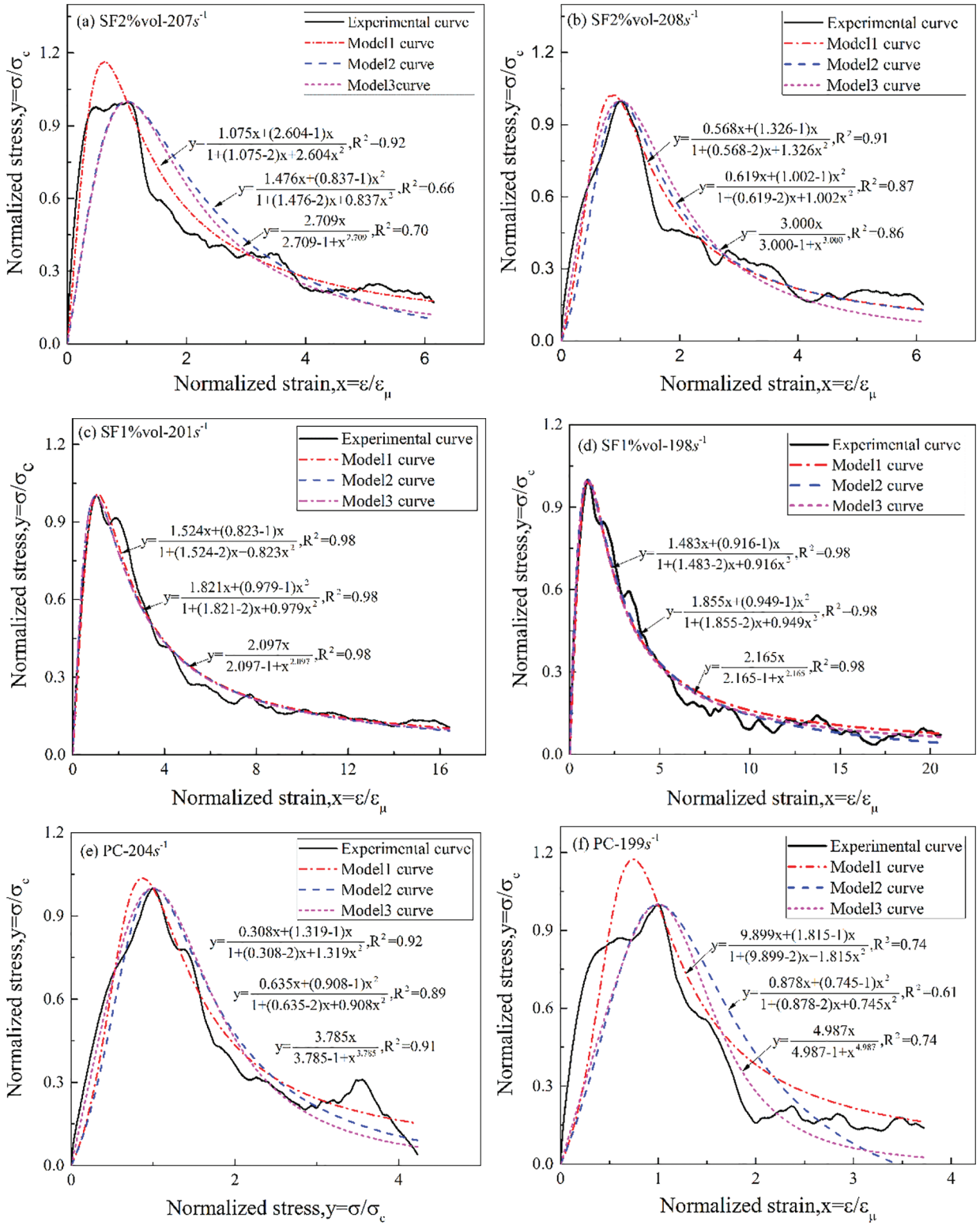

Figure 15: Dynamic stress-strain curve models of SFRCCs composites

Table 9: Validation and evaluation of stress-strain models

Specimen	Model	Slope and curvature of normalized stress-strain curves				Evaluation results
		x = 0		x = 1		
		$\left(\frac{dy}{dx}\right) > 0$	$\left(\frac{dy^2}{dx^2}\right) \leq 0$	$\left(\frac{dy}{dx}\right) = 0$	$\left(\frac{dy^2}{dx^2}\right) < 0$	
SF2%vol-207 s^{-1}	1	2.679	4.956	-0.599	-0.030	NO
	2	1.476	2.899	0	−1.523	NO
	3	1.585	0	0	−1.709	YES
SF2%vol−208 s^{-1}	1	0.894	2.560	−0.365	−1.971	NO
	2	0.619	1.238	0	−3.220	NO
	3	1.5	0	0	−2	YES
SF1%vol−201 s^{-1}	1	1.347	1.282	0.131	−1.450	NO
	2	1.821	3.641	0	−1.111	NO
	3	1.912	0	0	−1.097	YES
SF1%vol−198 s^{-1}	1	1.399	1.447	0.060	−1.422	NO
	2	1.855	3.705	0	−1.109	NO
	3	1.858	0	0	−1.165	YES
PC−199 s^{-1}	1	0.627	2.122	−0.509	−2.672	NO
	2	0.635	1.253	0	−3.683	NO
	3	1.359	0	0	−2.785	YES
PC−204 s^{-1}	1	10.714	−169.26	−0.076	−0.175	NO
	2	0.878	1.626	0	−3.210	NO
	3	1.251	0	0	−3.987	YES

Note: "YES" and "NO" mean that the calculated parameters satisfy or not the essential requirements of the model.

4 Conclusions

In this paper, the effects of strain rate and fiber content on the dynamic mechanical behavior of SFRCCs were considered by using an SHPB device. The complete dynamic stress-strain curves and energy integrals were obtained. Moreover, scanning electron microscopy (SEM) and energy-dispersive X-ray spectrometry (EDS) were applied to explore the fiber strengthening and toughening mechanism of the cement matrix at the microscale. In addition, three analytical models of SFRCCs were proposed to describe the complete stress-strain responses of sisal fibers reinforced cement composites, and the obtained parameters were evaluated in the context of the mathematical boundary conditions. Based on the findings of this study, the following conclusions can be drawn:

(1) Compared with OCCs, the addition of sisal fibers can improve the dynamic mechanical properties of cement-based composites to a certain extent. When the fiber content exceeds 1% vol, the peak stress does not increase further, but the ultimate strain and energy integral are significantly enhanced with increasing fiber content.

(2) SFRCCs are sensitive to the dynamic strain rate. A higher strain rate significantly improves the peak stress, ultimate strain, and energy integrals of the composites. The size of the fragments decreases with increasing impact velocity, as there is more energy absorbed.
(3) The introduction of sisal fibers into the cement-based composites changes their damage failure mode. For OCCs, the failure mode was the brittle fracture of the crystal structure plane and cavities. In contrast, the failure mode of the SFRCCs changes from brittleness to ductility, as illustrated by the microcrack propagation from fiber pull-out holes to voids, multi-interface debonding, and the mechanical interlocking caused by roughness.
(4) Three models were investigated to properly describe the stress-strain curves of the cement-based composites, and their effectiveness was verified based on strict mathematical boundary conditions. Only one of those models (model 3) was found to meet them. According to the fitting results of model 3, the fitting coefficient directly reflects the influence of fiber content on the peak stress. That is, the higher fiber content yields a smaller fitting coefficient and the greater composite peak stress.
(5) The dynamic compression mechanical properties of the SFRCCs under high strain rates were discussed, and the influence of fiber content and strain rate on the dynamic mechanical properties and the corresponding mechanisms were preliminarily discussed. The results reported herein are expected to provide a technical basis for the further preparation and engineering application of SFRCCs.

Funding Statement: This work was supported within the framework of the Basic Research Project of the Yunnan Province-Young Program (No. 2019FD097); Agricultural Joint Special Project of the Yunnan Province-General Program (No. 202101BD070001–118).

Conflicts of Interest: The authors declare that they have no conflicts of interest to report regarding the present study.

References

1. Onuaguluchi, O., Banthia, N. (2016). Plant-based natural fibre reinforced cement composites: A review. *Cement and Concrete Composites, 68,* 96–108. DOI 10.1016/j.cemconcomp.2016.02.014.
2. Khan, U. A., Jahanzaib, H. M., Khan, M., Ali, M. (2018). Improving the tensile energy absorption of high strength natural fiber reinforced concrete with fly-ash for bridge girders. *Key Engineering Materials, 765,* 335–342. DOI 10.4028/www.scientific.net/KEM.765.335.
3. Wang, B., Yan, L., Kasal, B. (2022). A review of coir fibre and coir fibre reinforced cement-based composite materials (2000–2021). *Journal of Cleaner Production, 338*. DOI 10.1016/j.jclepro.2022.130676.
4. Laverde, V., Marin, A., Benjumea, J. E. M., Ortiz, M. R. (2022). Use of vegetable fibers as reinforcements in cement-matrix composite materials: A review. *Construction and Building Materials, 340*. DOI 10.1016/j.conbuildmat.2022.127729.
5. Xie, C., Cao, M., Guan, J., Liu, Z., Khan, M. (2021). Improvement of boundary effect model in multi-scale hybrid fibers reinforced cementitious composite and prediction of its structural failure behavior. *Composites Part B: Engineering, 224*. DOI 10.1016/j.compositesb.2021.109219.
6. Xie, C., Cao, M., Si, W., Khan, M. (2020). Experimental evaluation on fiber distribution characteristics and mechanical properties of calcium carbonate whisker modified hybrid fibers reinforced cementitious composites. *Construction and Building Materials, 265*. DOI 10.1016/j.conbuildmat.2020.120292.
7. Benaimeche, O., Seghir, N. T., Sadowski, Ł, Mellas, M. (2020). The utilization of vegetable fibers in cementitious materials. *Encyclopedia of Renewable and Sustainable Materials, 2,* 649–662. DOI 10.1016/b978-0-12-803581-8.11596-6.
8. Li, Y., Li, Q. (2017). High mechanical performance and multifunctionalizations of plant fiber reinforced composites. *Chinese Journal of Solid Mechanics, 38(3),* 215–243. DOI 10.19636/j.cnki.cjsm42-1250/o3.2017.03.002.

9. Liang, X., Yang, G., Zeng, H. (2005). Researeh progres sof short sisal fiber reinforced composites. *Materials Reports, 2,* 63–66. DOI 10.3321/j.issn:1005-023X.2005.02.019.
10. Veigas, M. G., Najimi, M., Shafei, B. (2022). Cementitious composites made with natural fibers: Investigation of uncoated and coated sisal fibers. *Case Studies in Construction Materials, 16*. DOI 10.1016/j.cscm.2021.e00788.
11. Filho, A., Parveen, S., Rana, S., Vanderlei, R., Fangueiro, R. (2020). Mechanical and micro-structural investigation of multi-scale cementitious composites developed using sisal fibres and microcrystalline cellulose. *Industrial Crops and Products, 158*. DOI 10.1016/j.indcrop.2020.112912.
12. Ren, G., Yao, B., Ren, M., Gao, X. (2022). Utilization of natural sisal fibers to manufacture eco-friendly ultra-high performance concrete with low autogenous shrinkage. *Journal of Cleaner Production, 332*. DOI 10.1016/j.jclepro.2021.130105.
13. Shah, I., Li, J., Yang, S., Zhang, Y., Anwar, A. (2022). Experimental investigation on the mechanical properties of natural fiber reinforced concrete. *Journal of Renewable Materials, 10(5),* 1307–1320. DOI 10.32604/jrm.2022.017513.
14. Wang, C., Zhi, Z., Ren, Z., Sheraz, H., Wang, W. et al. (2018). Effects of rice husk fiber particle size and content on the properties of cement composites. *Journal of Composites, 35(6),* 1582–1589. DOI 10.13801/j.cnki.fhclxb.20170824.005.
15. Naraganti, S. R., Pannem, R. M. R., Putta, J. (2019). Impact resistance of hybrid fibre reinforced concrete containing sisal fibres. *Ain Shams Engineering Journal, 10(2),* 297–305. DOI 10.1016/j.asej.2018.12.004.
16. Sabarish, K. V., Paul, P., Bhuvaneshwari, J. J. (2020). An experimental investigation on properties of sisal fiber used in the concrete. *Materials Today: Proceedings, 22,* 439–443. DOI 10.1016/j.matpr.2019.07.686.
17. Do, J., Nie, H., Yan, Y., Wang, Y., Du, Y. (2016). Study on mechanical properties of sisal fiber reinforced self compacting lightweight aggregate concrete. *New Building Materials, 43(8),* 89–91.
18. Huo, J., Ren, X., Xiao, Y. (2012). Experimental study on drop weight dynamic impact of concrete filled steel tubular short columns under standard fire. *Journal of Civil Engineering, 4,* 9–20. DOI 10.15951/j.tmgcxb.2012.04.009.
19. Zhang, F., Shedbale, A. S., Zhong, R., Hien, P. L., Zhang, M. (2021). Ultra-high performance concrete subjected to high-velocity projectile impact: Implementation of K&C model with consideration of failure surfaces and dynamic increase factors. *International Journal of Impact Engineering, 155*. DOI 10.1016/j.ijimpeng.2021.103907.
20. Liu, J., Li, J., Fang, J., Su, Y., Wu, C. (2022). Ultra-high performance concrete targets against high velocity projectile impact–A-state-of-the-art review. *International Journal of Impact Engineering, 160*. DOI 10.1016/j.ijimpeng.2021.104080.
21. Zhong, H., Zhang, M. (2022). Effect of recycled polymer fibre on dynamic compressive behaviour of engineered geopolymer composites. *Ceramics International*. DOI 10.1016/j.ceramint.2022.05.023.
22. Xiao, S., Liao, S., Zhong, G., Guo, Y., Lin, J. et al. (2021). Dynamic properties of PVA short fiber reinforced low-calcium fly ash–slag geopolymer under an SHPB impact load. *Journal of Building Engineering, 44*. DOI 10.1016/j.jobe.2021.103220.
23. Chen, W., Guo, Z., Zou, H., Zhang, T. (2017). Experimental study on resistance of steel pipe RPC columns to short-range explosion load after standard fire. *Engineering Mechanics, 34(1),* 180–191. DOI 10.6052/j.issn.1000-4750.2015.07.0537.
24. Huang, B., Xiao, Y. (2020). Compressive impact tests of lightweight concrete with 155-mm-diameter spilt hopkinson pressure bar. *Cement and Concrete Composites, 114*. DOI 10.1016/j.cemconcomp.2020.103816.
25. Trindade, A. C. C., Heravi, A. A., IurieCurosu, L. M., Silva, F. D. A. (2020). Tensile behavior of strain-hardening geopolymer composites (SHGC) under impact loading. *Cement and Concrete Composites, 113*. DOI 10.1016/j.cemconcomp.2020.103703.
26. Abadel, A., Al-Salloum, Y., Abbas, H., Siddiqui, N., Almusallam, T. (2016). Mechanical properties of hybrid fibre-reinforced concrete–Analytical modelling and experimental behaviour. *Magazine of Concrete Research, 68(16),* 823–843. DOI 10.1680/jmacr.15.00276.
27. Cao, M., Liu, Z., Xie, C. (2020). Effect of steel-PVA hybrid fibers on compressive behavior of $CaCO_3$ whiskers reinforced cement mortar. *Journal of Building Engineering, 31*. DOI 10.1016/j.jobe.2020.101314.

28. Khan, M., Cao, M., Xie, C., Ali, M. (2022). Effectiveness of hybrid steel-basalt fiber reinforced concrete under compression. *Case Studies in Construction Materials, 16*. DOI 10.1016/j.cscm.2022.e00941.
29. Zhang, Y., Guo, R., Xia, H., Yan, F., Liu, X. (2021). Research on dynamic mechanical behavior and damage evolution mechanism of Cu/WCp laminated composites. *Materials Research Express, 8(1)*. DOI 10.1088/2053-1591/abda6a.
30. Zheng, M., He, D., Chen, F. (2001). Compressive stress-strain characteristics and energy absorption properties of porous aluminum alloys. *Chinese Journal of Nonferrous Metals, 11,* 81–85. DOI 10.19476/j.ysxb.1004.0609.2001.s2.018.
31. Zhang, H., Wang, B., Xie, A., Qi, Y. (2017). Experimental study on dynamic mechanical properties and constitutive model of basalt fiber reinforced concrete. *Construction and Building Materials, 152,* 154–167. DOI 10.1016/j.conbuildmat.2017.06.177.
32. Andic-Cakir, O., Sarikanat, M., Tuefekci, H. B., Demirci, C., Erdogan, U. H. (2014). Physical and mechanical properties of randomly oriented coir fiber–Cementitious composites. *Composites Part B: Engineering, 61,* 49–54. DOI 10.1016/j.compositesb.2014.01.029.
33. Tonoli, H., Belgacem, M., Siqueira, G., Bras, J., Lahr, F. (2013). Processing and dimensional changes of cement based composites reinforced with surface-treated cellulose fibres. *Cement & Concrete Composites, 37(3),* 68–75. DOI 10.1016/j.cemconcomp.2012.12.004.
34. Guo, Z. (1997). *Strength and deformation of concrete: Experimental basis and constitutive model*. Beijing, China: Tsinghua University Press.